PHYSICAL REVIEW E **67**, 031706 (2003)

Optically induced dynamics in nematic liquid crystals: The role of twist deformation and asymmetry

E. Brasselet*
Laboratoire de Photonique Quantique et Moléculaire, Ecole Normale Supérieure de Cachan, 94235 Cachan Cedex, France

B. Doyon and T. V. Galstian†
Département de Physique, de Génie Physique, et d'Optique, Université Laval, Cité Universitaire, Québec, Canada G1K 7P4

L. J. Dubé‡
Laboratoire de Dynamique des Ions, des Atomes, et des Molécules, Université Pierre et Marie Curie, 4 Place Jussieu, 75252 Paris Cedex 05, France

(Received 10 September 2002; published 26 March 2003)

We present a theoretical study of optically induced dynamics in a homeotropic nematic liquid crystal excited at normal incidence. By retaining the first symmetric and antisymmetric reorientation modes, the dynamical equations are reduced to a four-dimensional problem. The main advantage of this *minimal* approach is to emphasize the role of twisted mode and asymmetry of the light-induced molecular reorientation in a manner suitable for a clear physical interpretation. Theoretical results are compared with experiments in the particular case of circularly polarized light beams to show the physical origin of mode competition and of the breakdown of chiral and longitudinal symmetry. The model successfully describes previous experimental studies such as time-dependent three-dimensional molecular dynamics, light-induced stabilized helical reorientation, and in-plane precession regime in achiral nematics. While a recent experiment has revealed a new spatiotemporal transition, the model succeeds to describe all the features of such a bifurcation pointing out anew the importance of asymmetry. Finally, the first quantitative description of the appearance of a giant mirrorless optical bistability when twisted reorientation modes are excited is demonstrated. A qualitative physical interpretation is suggested for all these phenomena.

DOI: 10.1103/PhysRevE.67.031706 PACS number(s): 42.70.Df, 42.65.−k, 61.30.Gd

I. INTRODUCTION

The nonlinear optics of liquid crystals may be considered today as a well-established research field [1–4]. The rich nature of corresponding physical phenomena includes light-induced isothermal phase transitions [1,5,6], beam coupling and stimulated scattering [7], bistability [8,9]. Despite a large number of studies, however, many key questions remain unanswered. Among these questions, the physical origins of light-induced abrupt transitions between dynamic oscillations and of the strong self-diffraction regimes must still be clarified. Namely, many theoretical and simulation studies [10–15] have succeeded in retrieving the main features of observed phenomena, while the corresponding *physical* interpretations are still incomplete. In this regard, the relatively simple case of the normally incident light with elliptical polarization on a homeotropic cell of nematic liquid crystal (NLC) has received particular attention. The rich variety of dynamical regimes, observed experimentally [10], has been the subject of further theoretical studies and important progress has recently been achieved [16]. In parallel to these studies, our group has been focusing on the nature of the physical phenomena that define the transitions between different dynamical regimes [17–19]. We have followed the previous theoretical assumptions that the twist deformations should be present in the excitation spectrum [20] and we have identified a number of abrupt transitions, which are directly related to the breakdown of symmetry at particular points in the system [17–19]. For instance, our experimental observations have suggested that the breakdown of the chiral symmetry of the system, via the formation of twisted excitation modes, and their competition (for energy repartition) with polar deformations should be at the origin of the important fluctuations and the transitions to the strong self-diffraction regime [17]. Further experimental results and theoretical studies have confirmed these assumptions [18,19].

Another new abrupt transition, observed in the same geometry has brought us to the suggestion that, again, the breakdown of the symmetry via the formation of asymmetrical longitudinal modes and their competition with the symmetric ones, should be responsible for this transition [21]. In the present work, we develop a theoretical model, which provides the corresponding mathematical description of these two phenomena and appears to be in a very good agreement with experimental observations confirming the assumptions mentioned above. Specifically, we choose to discuss results of the present model for the case of the circularly polarized light excitation (instead of the general case of elliptically

*Corresponding author. Email address: ebrassel@lpqm.ens-cachan.fr

†Also at the Center d'Optique, Photonique, et Laser, Université Laval, Québec, Canada; Photintech Inc., 1245 Chemin Ste-Foy, Québec, Canada.

‡Also at Département de Physique, de Génie Physique, et d'Optique, Université Laval, Cité Universitaire, Québec, Canada G1K 7P4.

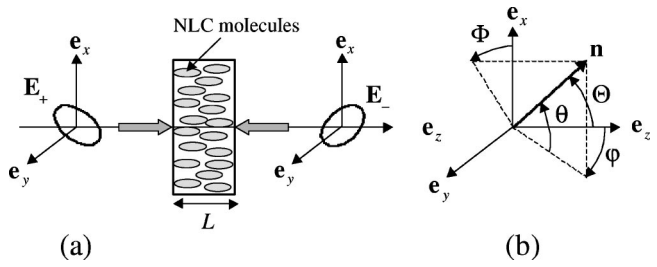

FIG. 1. (a) Interaction geometry. (b) Definition of the director $\boldsymbol{n}$ (on the right). $\boldsymbol{E}_+$ is the light wave propagating towards $z>0$ and $\boldsymbol{E}_-$ is the wave propagating towards $z<0$. L is the thickness of the nematic film and $\{\boldsymbol{e}_x,\boldsymbol{e}_y,\boldsymbol{e}_z\}$ is the Cartesian coordinate system. Two representations of the director's orientation are illustrated using (θ,ϕ) and (Θ,Φ) where $\theta=\angle(\boldsymbol{n}-\boldsymbol{n}_x,\boldsymbol{n})$, $\phi=\angle(\boldsymbol{e}_z,\boldsymbol{n}-\boldsymbol{n}_x)$, $\Theta=\angle(\boldsymbol{e}_z,\boldsymbol{n})$, and $\Phi=\angle(\boldsymbol{e}_x,\boldsymbol{n}-\boldsymbol{n}_z)$.

polarized light) to show clearly the physical roles of chiral and longitudinal symmetry breakdown and mode competition at the origin of the phenomena discussed. The physical results obtained compensate largely for the loss of generality in considering this particular case.

The paper is constructed as follows. Section II sums up the theoretical background that leads to a *minimal model* that will subsequently be used to account for a wide range of experimental observations. The physical content of the model is geared to elucidate the role played by the twist deformations and the asymmetry of the molecular orientations on the observed dynamics. Under different excitation regimes, the next three sections examine various facets of the optically induced dynamics. Section III covers some aspects of the *three-dimensional dynamics* of the director whereas Sec. IV describes a new *bifurcation induced by asymmetrical modes of excitation* and Sec. V explains *optical bistability as largely driven by twist deformations*. In these sections, the presentation iterates an identical scheme: the experimental evidences are reviewed, a quantitative confrontation with the theoretical predictions of the minimal model is displayed, and a physical interpretation of the observed phenomena is proposed. Finally, our conclusions are summarized in Sec. VI together with prospective comments on possible theoretical improvements.

II. THEORETICAL MODEL

A. Equations of motion

We study the light matter interaction between excitation beams normally incident on a NLC film sandwiched between two parallel glass substrates chemically treated to provide strong homeotropic alignment, i.e., the molecules in the neighborhood of the substrate are perpendicular to it (Fig. 1). We choose a Cartesian coordinate system (x,y,z) with the z axis being the direction of the propagation of light (Fig. 1). The average local orientation of the molecules is defined by the unit vector $\boldsymbol{n}$, called *director*, whose orientation may be given by the two angles (θ,ϕ) or (Θ,Φ) (the usual spherical angles), namely, $\boldsymbol{n}=(\sin\theta,\cos\theta\sin\phi,\cos\theta\cos\phi)$ in the first representation and $\boldsymbol{n}=(\sin\Theta\cos\Phi,\sin\Theta\sin\Phi,\cos\Theta)$ in the second (Fig. 1). We will further refer to either one of these two representations when comparing the model to experiments, however, the theory, presented in this section, is based on the (θ,ϕ) representation. We use the infinite plane wave approximation, which is justified experimentally if the spot sizes of the excitation beams are significantly larger than the thickness L of the NLC film. Under this assumption, all the functions will only depend on the spatial coordinate z and time t. The total real electric field of light is written as $\boldsymbol{E}_{\text{real}}(z,t)=1/2[\boldsymbol{E}(z,t)\mathrm{e}^{-i\omega t}+\text{c.c.}]$, where $\boldsymbol{E}=\boldsymbol{E}_++\boldsymbol{E}_-$ is the complex representation of the total electric field obtained from the superposition of the counterpropagating light waves (see Fig. 1) and ω is the frequency of light. Finally, the strong anchoring conditions $[\theta(0,t)=\theta(L,t)=\phi(0,t)=\phi(L,t)=0]$ allow to expand the angles θ and ϕ as Fourier series,

$$\theta(z,t)=\sum_{n=1}^{\infty}\theta_n(t)\sin(n\pi z/L),$$

$$\phi(z,t)=\sum_{n=1}^{\infty}\phi_n(t)\sin(n\pi z/L).$$

The dynamical equations of motion for the director under the action of a light field are obtained by writing the balance of torque between the elastic $\boldsymbol{\Gamma}_{\text{el}}$, electromagnetic $\boldsymbol{\Gamma}_{\text{em}}$, and viscous $\boldsymbol{\Gamma}_{\text{visc}}$ torques, namely, $\Gamma_{\text{el},\alpha}+\Gamma_{\text{em},\alpha}+\Gamma_{\text{visc},\alpha}=0$, where $\alpha=\theta$ or $\alpha=\phi$ [1]. These torques are calculated from elastic and electromagnetic free energy densities, respectively, F_{el} and F_{em}, and the dissipation function density R, using a variational principle [1]. F_{el} is given in Ref. [22] as

$$F_{\text{el}}=\frac{1}{2}K_1(\boldsymbol{\nabla}\cdot\boldsymbol{n})^2+\frac{1}{2}K_2(\boldsymbol{n}\cdot\boldsymbol{\nabla}\times\boldsymbol{n})^2+\frac{1}{2}K_3(\boldsymbol{n}\times\boldsymbol{\nabla}\times\boldsymbol{n})^2, \tag{1}$$

where K_1, K_2, and K_3 are the Frank elastic constants associated with splay, twist, and bend deformations of the director, respectively. To be specific, we will use the ratios $K_1/K_3=2/3$ and $K_2/K_3=1/2$, valid for the nematic liquid crystal $E7$ used in our experiments. Then using

$$\Gamma_{\text{el},\alpha}=\frac{\partial}{\partial z}\left(\frac{\partial F_{\text{el}}}{\partial(\partial\alpha/\partial z)}\right)-\frac{\partial F_{\text{el}}}{\partial\alpha}$$

and the definitions

$$\Gamma_{\text{el},\theta}\equiv K_3\overline{\Gamma}_{\text{el},\theta},\quad \Gamma_{\text{el},\phi}\equiv K_3\cos^2\theta\,\overline{\Gamma}_{\text{el},\phi}, \tag{2}$$

we obtain

$$\overline{\Gamma}_{\text{el},\theta}=a_{\text{el}1}\theta_{zz}+a_{\text{el}2}\phi_{zz}+a_{\text{el}3}\theta_z^2+a_{\text{el}4}\theta_z\phi_z+a_{\text{el}5}\phi_z^2,$$

$$\overline{\Gamma}_{\text{el},\phi}=b_{\text{el}1}\theta_{zz}+b_{\text{el}2}\phi_{zz}+b_{\text{el}3}\theta_z^2+b_{\text{el}4}\theta_z\phi_z+b_{\text{el}5}\phi_z^2,$$

where the partial derivatives are abbreviated by an index notation and the coefficients $a_{\text{el}i}$ and $b_{\text{el}i}$ are given by

$$a_{\text{el}1}=1-\frac{1}{2}\sin^2\phi-\frac{1}{3}\sin^2\theta\cos^2\phi,$$

$$a_{\mathrm{el2}}=\frac{1}{24}\sin 2\theta\sin 2\phi,$$

$$a_{\mathrm{el3}}=-\frac{1}{6}\sin 2\theta\cos^2\phi,$$

$$a_{\mathrm{el4}}=-\frac{1}{6}\sin 2\phi(1+2\cos^2\theta),$$

$$a_{\mathrm{el5}}=\frac{1}{4}\sin 2\theta\left(1+\frac{1}{3}\cos^2\phi+2\cos^2\theta\cos^2\phi\right), \tag{3}$$

$$b_{\mathrm{el1}}=\frac{1}{12}\tan\theta\sin 2\phi,$$

$$b_{\mathrm{el2}}=\frac{1}{2}\left(1+\frac{1}{3}\sin^2\phi+\cos^2\theta\cos^2\phi\right),$$

$$b_{\mathrm{el3}}=\frac{1}{3}\sin 2\phi,$$

$$b_{\mathrm{el4}}=-\tan\theta\left(1+\frac{1}{3}\sin^2\phi+2\cos^2\theta\cos^2\phi\right),$$

$$b_{\mathrm{el5}}=\frac{1}{12}\sin 2\phi(1-3\cos^2\theta).$$

Neglecting the magnetic anisotropy, F_{em} may be defined as [23]

$$F_{\mathrm{em}}=-\frac{1}{16\pi}\sum_{i,j}\epsilon_{ij}E_iE_j^*, \tag{4}$$

where $\epsilon_{ij}=\epsilon_\perp\delta_{ij}+\epsilon_a n_i n_j$ is the dielectric constant, $\epsilon_a=\epsilon_\parallel-\epsilon_\perp$ is the dielectric anisotropy, and δ_{ij} is the Kronecker symbol. Using $\nabla\cdot(\boldsymbol{\epsilon E})=0$, the expression

$$\Gamma_{\mathrm{em},\alpha}=\frac{\partial}{\partial z}\left(\frac{\partial F_{\mathrm{em}}}{\partial(\partial\alpha/\partial z)}\right)-\frac{\partial F_{\mathrm{em}}}{\partial\alpha}$$

and the definitions

$$\Gamma_{\mathrm{em},\theta}\equiv\frac{\epsilon_a}{16\pi}\overline{\Gamma}_{\mathrm{em},\theta},\quad \Gamma_{\mathrm{em},\phi}\equiv\frac{\epsilon_a}{16\pi}\cos^2\theta\overline{\Gamma}_{\mathrm{em},\phi} \tag{5}$$

allows us to write

$$\overline{\Gamma}_{\mathrm{em},\theta}=\frac{\sin 2\theta}{(1+\eta\cos^2\theta\cos^2\phi)^2}[a_{\mathrm{em1}}|E_x|^2+a_{\mathrm{em2}}|E_y|^2+a_{\mathrm{em3}}(E_xE_y^*+E_x^*E_y)],$$

$$\overline{\Gamma}_{\mathrm{em},\phi}=\frac{\sin 2\phi}{(1+\eta\cos^2\theta\cos^2\phi)^2}[b_{\mathrm{em1}}|E_x|^2+b_{\mathrm{em2}}|E_y|^2+b_{\mathrm{em3}}(E_xE_y^*+E_x^*E_y)],$$

with coefficients $a_{\mathrm{em}i}$ and $b_{\mathrm{em}i}$ given by

$$a_{\mathrm{em1}}=1+\eta\cos^2\phi,$$

$$a_{\mathrm{em2}}=-\sin^2\phi,$$

$$a_{\mathrm{em3}}=\sin\phi\left(\cot 2\theta+\frac{\eta}{2}\cot\theta\cos^2\phi\right), \tag{6}$$

$$b_{\mathrm{em1}}=\eta\sin^2\theta,$$

$$b_{\mathrm{em2}}=1+\eta\cos^2\theta,$$

$$b_{\mathrm{em3}}=\frac{\tan\theta}{2\sin\phi}[1+\eta\cos^2\theta(1+\sin^2\phi)],$$

and where we have introduced the parameter $\eta=\epsilon_a/\epsilon_\perp$. Finally, in the absence of velocity field for the director, R is taken as [22]

$$R=\frac{1}{2}\gamma\left(\frac{\partial\boldsymbol{n}}{\partial t}\right)^2, \tag{7}$$

where γ is the orientational viscosity. Then, using

$$\Gamma_{\mathrm{visc},\alpha}=-\frac{\partial R}{\partial(\partial\alpha/\partial t)}$$

we obtain

$$\Gamma_{\mathrm{visc},\theta}=-\gamma\frac{\partial\theta}{\partial t},\quad \Gamma_{\mathrm{visc},\phi}=-\gamma\cos^2\theta\frac{\partial\phi}{\partial t}. \tag{8}$$

By projecting the balance of torques on each mode θ_n and ϕ_n, we obtain the dynamical equations for the amplitudes α_n (i.e., θ_n or ϕ_n):

$$\tau\frac{\partial\alpha_n}{\partial t}=\int_0^1 d\xi\sin(n\pi\xi)\left[\frac{2}{\pi^2}\overline{\Gamma}_{\mathrm{el},\alpha}(\xi,t)+\frac{(1+\eta)}{I_{\mathrm{lin}}}\overline{\Gamma}_{\mathrm{em},\alpha}(\xi,t)\right], \tag{9}$$

where we have introduced a normalized length $\xi=z/L$, a characteristic orientation time for the cell $\tau=\gamma L^2/(K_3\pi^2)$ (typically for $L=100$ μm, $\tau\sim 10$ sec) and the intensity $I_{\mathrm{lin}}=8\pi^3K_3\epsilon_\parallel/(\epsilon_a\epsilon_\perp L^2)$ that corresponds to the Fréedericksz transition for a linearly polarized excitation light [23]. In order to solve numerically Eqs. (9), it is necessary to know the electric field in the nematic film. In the following section, the Maxwell equations that take into account the director's reorientation are used to obtain the expression of the electric field.

B. Light propagation

The propagation of light through the reoriented NLC is treated using Berreman's formalism where Maxwell equations are written in the form [24]

$$\frac{d\Psi}{dz}=ik_0\boldsymbol{D}\Psi \tag{10}$$

with

$$\Psi=\begin{pmatrix} E_x \\ H_y \\ E_y \\ -H_x \end{pmatrix} \tag{11}$$

and

$$\boldsymbol{D}=\begin{pmatrix} 0 & 1 & 0 & 0 \\ \epsilon_{xx}-\dfrac{\epsilon_{xz}^2}{\epsilon_{zz}} & 0 & \epsilon_{xy}-\dfrac{\epsilon_{xz}\epsilon_{yz}}{\epsilon_{zz}} & 0 \\ 0 & 0 & 0 & 1 \\ \epsilon_{xy}-\dfrac{\epsilon_{xz}\epsilon_{yz}}{\epsilon_{zz}} & 0 & \epsilon_{yy}-\dfrac{\epsilon_{yz}^2}{\epsilon_{zz}} & 0 \end{pmatrix}. \tag{12}$$

Let us introduce the wave vector in the absence of reorientation, $\kappa=k_0\sqrt{\epsilon_\perp}$, where $k_0=\omega/c$ is the wave vector in vacuum. When the NLC is distorted, we obtain from Eqs. (10) and (11) that the propagation of the electric field $\boldsymbol{E}$ is given by the following set of coupled equations for its x and y components:

$$\frac{d^2E_j}{dz^2}=-\kappa^2E_j-\kappa^2\eta(d_{jx}E_x+d_{jy}E_y) \quad (j=x,y), \tag{13}$$

where

$$d_{xx}=\frac{\sin^2\theta}{1+\eta\cos^2\theta\cos^2\phi},$$

$$d_{xy}=\frac{\sin\theta\cos\theta\sin\phi}{1+\eta\cos^2\theta\cos^2\phi}=d_{yx},$$

$$d_{yy}=\frac{\cos^2\theta\sin^2\phi}{1+\eta\cos^2\theta\cos^2\phi}.$$

The coefficients d_{jk} characterize the action of the director reorientation on the light propagation. Indeed, in absence of light the d_{jk} are zero ($\theta=\phi=0$) and Eq. (13) reduces to the propagation of light through an isotropic medium with refractive index $\sqrt{\epsilon_\perp}$. Thus, in the case of a light wave propagating towards $z>0$, we seek the electric field components in the form

$$E_{j+}(z)=[E_{j+}^0+E_{j+}^1(z)]e^{i\kappa z}\overline{E}_{j+}(z)e^{i\kappa z} \tag{14}$$

with $E_{j+}(0)=E_{j+}^0$. Then, using Eqs. (13) and (14) together with the boundary conditions $E_{x+}^1(z=0)=E_{y+}^1(z=0)=0$ and $(dE_{x+}^1/dz)_{z=0}=(dE_{y+}^1/dz)_{z=0}=0$, we obtain

$$E_{j+}^1(z)=i\frac{\kappa\eta}{2}\left\{\int_0^z[d_{jx}\overline{E}_{x+}(z')+d_{jy}\overline{E}_{y+}(z')]dz' - \int_0^z e^{2i\kappa(z'-z)}[d_{jx}\overline{E}_{x+}(z')+d_{jy}\overline{E}_{y+}(z')]dz'\right\}. \tag{15}$$

The first and the second term of the right-hand side of Eq. (15) give a contribution $\propto e^{+i\kappa z}$ and $\propto e^{-i\kappa z}$, respectively, to the field [see Eq. (14)]. They correspond to the incident and reflected waves, respectively. For slowly varying refractive index along the propagation direction ($|\theta_z|\ll 1/\lambda$ and $|\phi_z|\ll 1/\lambda$), the reflected wave can be neglected. This amounts to averaging to zero the second integral due to rapid oscillations of the term $e^{2i\kappa z}$ appearing in the integrand (for $\lambda\approx 0.5\ \mu$m, we have typically $\lambda/L\approx 10^{-2}$). The resulting differential equations are

$$\frac{dE_{j+}^1}{dz}=i\frac{\kappa\eta}{2}[d_{jx}\overline{E}_{x+}(z)+d_{jy}\overline{E}_{y+}(z)] \quad (j=x,y). \tag{16}$$

Similarly, for light wave propagating towards $z<0$, one assumes a form $E_{j-}(z)=[E_{j-}^0+E_{j-}^1(z)]e^{i\kappa(L-z)}$, with $E_{j-}(L)=E_{j-}^0$. The same procedure as above leads to a system of coupled equations analog to Eq. (16) with the change $\kappa\rightarrow-\kappa$.

C. A minimal model as a low excitation limit

The system of equations given by Eqs. (9) is integrated numerically together with Eqs. (14) and (16) for the x and y components of the electric field. However, Eqs. (9) are infinite dimensional, and one needs to truncate the series for θ and ϕ. In order to describe correctly the system in the simplest manner, we keep the first two modes of each angle, viz.,

$$\theta^{(2)}(\xi,t)=\theta_1(t)\sin(\pi\xi)+\theta_2(t)\sin(2\pi\xi), \tag{17}$$

$$\phi^{(2)}(\xi,t)=\phi_1(t)\sin(\pi\xi)+\phi_2(t)\sin(2\pi\xi). \tag{18}$$

This choice is the simplest that takes into account the asymmetry (with respect to $z=L/2$) of the molecular reorientation resulting from the asymmetric dielectric torque when the NLC film is reoriented. The dynamics of the system then reduces to the dependence of θ_1, θ_2, ϕ_1, and ϕ_2 on t and on the total incident intensity $I_{\rm tot}$. We choose to give these mode amplitudes as functions of the normalized time $\tilde{t}=t/\tau$ and the normalized intensity $\tilde{I}=I_{\rm tot}/I_F$, where I_F is the Fréedericksz threshold intensity. In the case of circularly polarized excitation beams $I_F=2I_{\rm lin}$ [1].

In order to perform the numerical integration of the coupled sets of ordinary differential equations (9) and (16) (initial value systems), we adopt the following procedure. For each value of t (alternatively $\tilde{t}$), the field equations (16) are integrated and stored on a mesh of points over the whole interval $z\in[0,L]$ (or $\xi\in[0,1]$) to provide input for the right-hand side of the angular equations (9). The mesh is chosen sufficiently fine to allow accurate interpolation for field am-

plitudes at z (or ξ) positions not available in the stored set. Each time the solutions of the angular equations are advanced in time, the field values are updated. We have found that an embedded fourth-order Cash-Karp Runge-Kutta algorithm with adaptive step size [25] produced stable results of high accuracy. The integrations were performed using $\epsilon_\perp = 2.28$ and $\epsilon_\parallel = 2.92$ which gives $\eta \approx 0.28$.

D. Towards a description of the twist deformation

Experimentally, a common way to obtain information about the molecular nonlinear dynamics is to measure the *shape* and *orientation* of the polarization ellipse $\mathcal{E}$ of the excitation beam or of a probe beam after it has passed through the reoriented region of the sample. Such measurements are possible when the polarization of light emerging from the sample is uniform over the transverse section of the beam when self-focusing effects are negligible, i.e., not too far above the Fréedericksz transition threshold. In the particular case of the adiabatic *Mauguin regime* of light propagation $(P(z)\Delta n(z) \gg \lambda$ where $P(z) = 2\pi/\partial_z \Phi$ is the local pitch of the helix formed by the director deformations and $\Delta n(z)$ is the local effective birefringence [26]), the shape of $\mathcal{E}$ is related to the overall amplitude of reorientation (i.e., Θ) whereas its orientation is associated to the position of the optical axis of the last slice traversed by the analyzed beam [i.e., $\Phi(L,t)$ and $\Phi(0,t)$ for a beam propagating towards $z > 0$ and $z < 0$, respectively]. To facilitate the ensuing discussion, we shall assume the validity of the adiabatic Mauguin propagation.

The shape of $\mathcal{E}$ is characterized by the light ellipticity, i.e., the angular momentum associated with a photon in units of $\hbar$. It is equal to $\cos\Delta$ where $\Delta \equiv \Delta(L,t)$ and $\Delta(z,t)$ is the light-induced phase shift between *e* and *o* waves for the light coming from $z < 0$ and passing through a slice of thickness z at the time t,

$$\Delta(z,t) = k_0 \int_0^z [n_e(z',t) - n_o] dz'$$

$$= \kappa \int_0^z \left[\sqrt{\frac{1+\eta}{1+\eta\cos^2\Theta}} - 1 \right] dz', \qquad (19)$$

where $n_e = \sqrt{\epsilon_\perp \epsilon_\parallel / \epsilon_{zz}}$ and $n_o = \sqrt{\epsilon_\perp}$ are the extraordinary and ordinary refractive indices, respectively. Thus Δ characterizes the amount of reorientation (see the definition of Θ, Fig. 1) and is given by

$$\Delta = \frac{4(1+\eta)}{\eta} \tilde{L} \int_0^1 \left[\sqrt{\frac{1+\eta}{1+\eta\cos^2\theta\cos^2\phi}} - 1 \right] d\xi, \quad (20)$$

where $\tilde{L} = (L/\lambda)[\pi \epsilon_a \epsilon_\perp^{1/2}/(2\epsilon_\parallel)]$ is the normalized length of the cell, which is, in a typical experiment, the length of the cell in micrometers (for $\epsilon_\perp = 2.28$, $\epsilon_\parallel = 2.92$, $\tilde{L} = 0.52L/\lambda$).

Concerning the orientation of $\mathcal{E}$, its principal axes are attached at $\pm 45°$ of the local optical axis position at the extremity of the cell when the incident light is circularly polarized. Thus, the angle $\mathcal{T}$ between the director orientations near the output $(z = L)$ and the input $(z = 0)$ planes of the cell,

$$\mathcal{T} = \Phi(L,t) - \Phi(0,t), \qquad (21)$$

characterizes the three-dimensional character of the director deformations [18] around the averaged plane of reorientation of the molecules defined by the angle $\bar{\Phi}$,

$$\bar{\Phi} = \frac{\Phi(0,t) + \Phi(L,t)}{2}. \qquad (22)$$

Finally, the instantaneous averaged angular velocity of the NLC film is given by

$$\Omega = \partial_t \bar{\Phi}. \qquad (23)$$

The expressions of $\mathcal{T}$ and Ω within the minimal model are obtained using the relation $\tan\Phi = \cot\theta \sin\phi$, which gives

$$\Phi^{(2)}(0,t) = \arctan\left(\frac{\phi_1 + 2\phi_2}{\theta_1 + 2\theta_2} \right), \qquad (24)$$

$$\Phi^{(2)}(L,t) = \arctan\left(\frac{\phi_1 - 2\phi_2}{\theta_1 - 2\theta_2} \right). \qquad (25)$$

For the sake of simplicity, we shall further refer to $\mathcal{T}$ as *twist*, keeping in mind, however, that if $\mathcal{T} = 0$, the spatial organization of the molecules in the bulk is not necessary in plane. Therefore, care must be exercised when comparing theory and experiment, since the light propagation is generally nonadiabatic such that the amplitude of reorientation (Θ) and the twisted molecular organization (Φ) are not directly connected with the measured ellipticity and the measured relative positions of the principal axes of $\mathcal{E}$.

III. THREE-DIMENSIONAL DYNAMICS

Let us define the three circularly polarized excitation light fields used in this work by

$$\mathrm{CP} \equiv \boldsymbol{E}_+ = E_0(\boldsymbol{e}_x + i\boldsymbol{e}_y), \quad \boldsymbol{E}_- = \boldsymbol{0},$$

$$\mathrm{CP}^{\pm} \equiv \boldsymbol{E}_+ = E_0(\boldsymbol{e}_x + i\boldsymbol{e}_y), \quad \boldsymbol{E}_- = E_0(\boldsymbol{e}_x - i\boldsymbol{e}_y)e^{i\delta(t)},$$

$$\mathrm{CP}^{+} \equiv \boldsymbol{E}_+ = E_0(\boldsymbol{e}_x + i\boldsymbol{e}_y), \quad \boldsymbol{E}_- = E_0(\boldsymbol{e}_x + i\boldsymbol{e}_y)e^{i\delta(t)}.$$

The phase factor $\exp[i \pm k_0 z - \omega t)]$ is omitted and a random phase $\delta(t)$ is added to represent the incoherence between the two superimposed light fields. In this way, the label CP refers to the case of a single circularly polarized excitation beam, the label $\mathrm{CP}^{\pm}$ corresponds to the case of two incoherent counterpropagating circularly polarized beams *with opposite angular momentum* and same intensity, and finally, the label CP^{+} amounts to the superposition of two incoherent counterpropagating circularly polarized beams *carrying the same angular momentum* and the same intensity.

In a previous study we have predicted theoretically that the three-dimensional light-induced dynamics could be con-

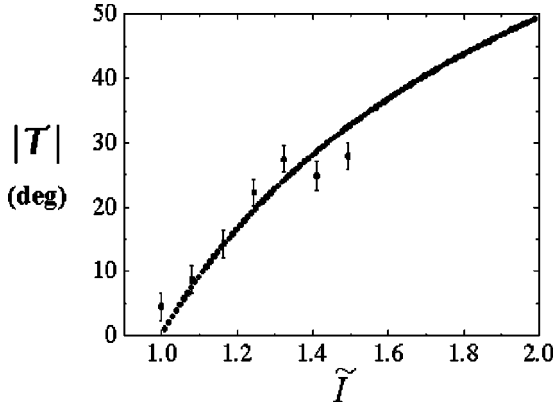

FIG. 2. Experimental (●) [18] and theoretical (full line) demonstration of the control of stationary twisted modes in the $CP^{\pm}$ case under the same operating conditions.

trolled using a two-beam technique [18]. It was shown in particular that the spatiotemporal behavior of the reoriented NLC film under CP, $CP^{\pm}$, and CP^{+} excitation should verify the following conditions:

$$\begin{aligned} &\mathrm{CP}: \Omega \neq 0, \quad \mathcal{T} \neq 0, \\ &\mathrm{CP}^{\pm}: \Omega = 0, \quad \mathcal{T} \neq 0, \\ &\mathrm{CP}^{+}: \Omega \neq 0, \quad \mathcal{T} = 0, \end{aligned} \tag{26}$$

where the angular velocity Ω and the twist $\mathcal{T}$ were *time independent* under the approximations used in Ref. [18]. Only qualitative agreement with experiments was found. For instance, in the CP case, a precessing ($\Omega \neq 0$) twisted ($\mathcal{T} \neq 0$) molecular configuration was indeed observed, but the configuration showed a *time-dependent* behavior. Also for the CP^{+} case, a quasi-in-plane ($\mathcal{T}=0$) precessing ($\Omega \neq 0$) reoriented configuration was identified, but it switched spontaneously to a stronger reorientation in a beam divergence regime where only one diffraction ring was observed. In the following, we provide a quantitative description of the experimental findings using the dynamical model presented in Sec. II.

A. Stationary twisted regime ($CP^{\pm}$)

Figure 2 shows the dependence of the measured twist, $\mathcal{T}_{\mathrm{expt}}$, versus the normalized intensity $\tilde{I}$ when the NLC is excited by the $CP^{\pm}$ field. Experimentally, the precession phenomenon is not observed ($\Omega=0$) and no significant variations of the reorientation amplitude (Δ) and of the twist ($\mathcal{T}$) are detected. Also shown in Fig. 2 is the prediction of the model for the twist deformation $\mathcal{T}$ according to Eq. (21). Despite the comments made at the end of Sec. II, it is clear that both theory and experiment agree on the signature of the twist deformation although the quantitative agreement may be considered more fortuitious.

The model also confirms the absence of precession together with a stationary reorientation amplitude and twist at fixed intensity ($\bar{\Phi}$, Δ, and $\mathcal{T}$ are constant). This behavior may be related to the efficiency of the spatial averaging of nonuniform angular momentum deposition inside the liquid crystal. As presented in Ref. [17], it is convenient to introduce the characteristic length of nonuniform light angular momentum, ℓ (see Fig. 3), and the electric coherence length, $\zeta = E^{-1}(4\pi K/\epsilon_a)^{1/2}$ [22], which is $\approx 10\ \mu$m in our case. Indeed, at the transition threshold, the symmetry is broken by reorientation of the liquid crystal molecules and the incident circular polarization becomes elliptical. The light deposits, therefore, angular momentum nonuniformly in the transparent medium. Figure 3 shows $m_X(\xi)$, the angular momentum deposition per photon and per unit of normalized length $\xi = z/L$, versus ξ calculated in the adiabatic approximation for $X=\mathrm{CP}$ and $X=\mathrm{CP}^{\pm}$ excitations. Using the balance of angular momentum in a slice of medium contained between the planes z and $z+dz$, one obtains

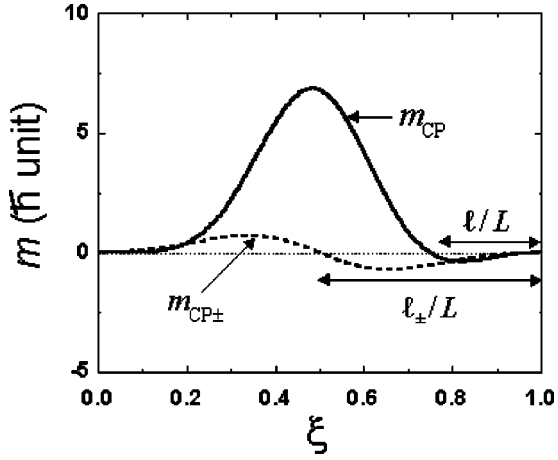

FIG. 3. Calculated angular momentum deposited per photon and per unit of normalized length $\xi = z/L$ vs ξ in the adiabatic approximation. m_{CP}, CP excitation; $m_{\mathrm{CP}^{\pm}}$, $CP^{\pm}$ excitation. $\Delta = 1.1\,\pi$ for the illustration.

$$\begin{aligned} m_{\mathrm{CP}}(\xi) &= -\hbar\,\partial_{\xi}\cos[\Delta u(\xi)], \\ m_{\mathrm{CP}^{\pm}}(\xi) &= [m_{\mathrm{CP}}(\xi) - m_{\mathrm{CP}}(1-\xi)]/2 \end{aligned} \tag{27}$$

for CP and $CP^{\pm}$, respectively, and where $u(\xi) = \xi - \sin(2\pi\xi)/(2\pi)$. When the excitation is $CP^{\pm}$, $\ell_{\pm} > \zeta$ and light-induced stabilized torsion takes place. This can be understood since the first part of the sample tends to rotate in one sense and the second part in the other sense independently until the elastic restoring torque compensates this torsion, leading to the stabilized twisted configuration presented in Fig. 2.

B. Dynamical twisted precession regime (CP)

Figure 4 displays the time behavior of the averaged plane of molecular reorientation $\bar{\Phi}_{\mathrm{expt}}$ and twist $\mathcal{T}_{\mathrm{expt}}$ observed above the Fréedericksz threshold in the case of a circularly polarized beam (CP). $\bar{\Phi}_{\mathrm{expt}}$ increases nearly linearly with time, indicating that a uniform precession regime takes place. This collective rotation of NLC molecules is associated with an oscillating three-dimensional (3D) reorientation. These observations are in good agreement with the predic-

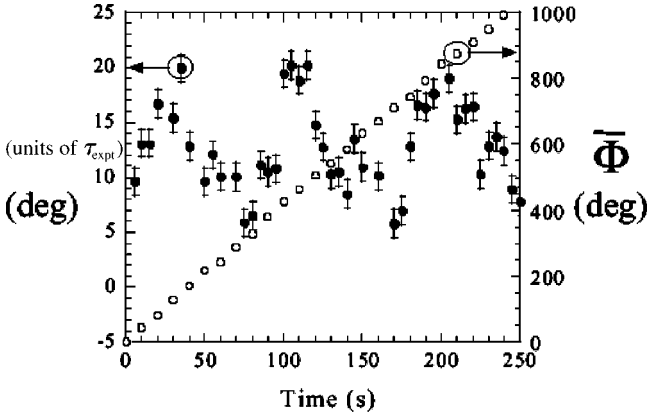

FIG. 4. Experimental demonstration of the torsional oscillation regime coupled with induced precession from Ref. [18] with CP excitation beam. $\tilde{I} \approx 1.1$ and the cell thickness is 90 μm. ○, twist $\mathcal{T}$; ●, position of the averaged plane of reorientation of the molecules $\bar{\Phi}$.

tion of the model as shown in Fig. 5 where $\bar{\Phi}$ has nearly a linear time dependence and $\mathcal{T}$ oscillates around a nonzero mean value. Moreover, the model predicts that the director precession is accompanied by a small nutation ($\partial_t \Delta \neq 0$) as reported earlier in several experimental studies [10,17,27]. The occurrence of such a time-dependent 3D behavior can be understood on the basis of the discussion done in Sec. III A.

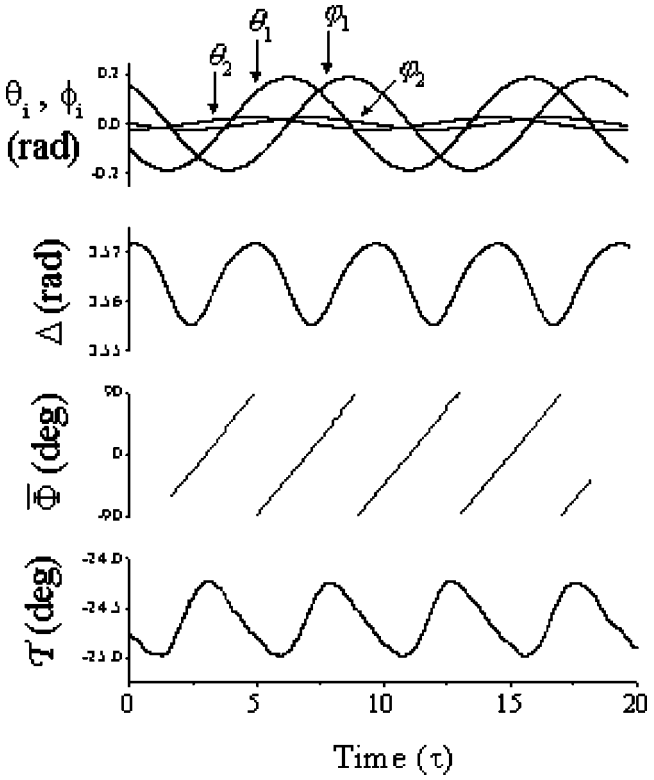

FIG. 5. Nonlinear dynamics calculated at $\tilde{I} = 1.3$ with CP excitation. The amplitudes θ_1, θ_2, ϕ_1, and ϕ_2, the position of the averaged plane of reorientation of the molecules $\bar{\Phi}$, the phase shift Δ, and the twist $\mathcal{T}$ are plotted vs time (in units of τ).

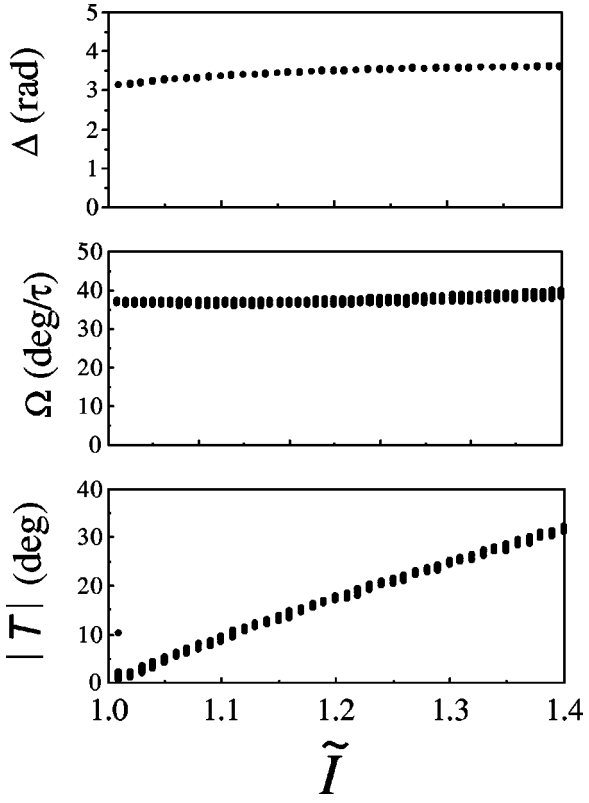

FIG. 6. Theoretical demonstration of the phase locking mechanism. The phase shift Δ, the precession rate Ω, and the twist $\mathcal{T}$ are plotted vs normalized intensity in the CP case.

Indeed, in the CP case, we see in Fig. 3 that ℓ is approximately equal to ζ (for a typical cell length L of 100 μm) and this allows us to foresee a not very efficient spatial averaging of the angular momentum deposition and therefore the appearance of undamped torsional oscillations.

The experimental study of the intensity dependence of the 3D dynamics, in the CP case, shows that the precession rate does not change significantly when the intensity is increased whereas the amplitude of the averaged twist increases appreciably [18]. This behavior is evidence of the underlying nature of an optical phase locking above the Fréedericksz threshold with the reorientation being frozen at $\Delta \approx \pi$ [5,20]. Figure 6 represents the calculated intensity dependence of the reorientation amplitude Δ, the precession rate Ω, and the twist $\mathcal{T}$. Increasing the intensity from $\tilde{I} = 1$ excites preferentially azimuthal deformations (Φ) over the polar ones (Θ) due to energy exchange between the *o* and the *e* waves. In summary, we observe a close quantitative agreement between theory and experiment.

C. In-plane precession regime (CP^+)

When the NLC film is reoriented under CP^+ excitation, just above the Fréedericksz transition, a transient quasi-in-plane uniform precession is observed before the system switches to a reorientation that corresponds to $\Delta \approx 2\pi - 3\pi$, since only one diffraction ring is observed [18]. Such a dynamics is well reproduced by the model as shown in Fig. 7.

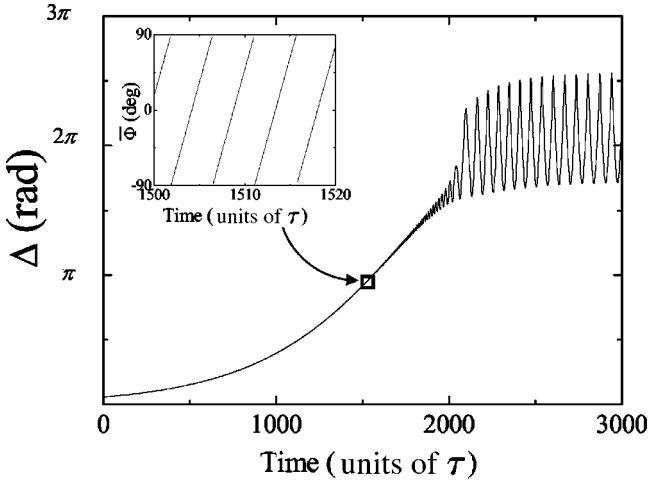

FIG. 7. Calculated Δ vs time in the CP^+ excitation case for $\tilde{I}=1.001$. Insets: demonstration of the quasiuniform precession regime when $\Delta \approx \pi$ and enlarged long-term behavior of Δ.

IV. ASYMMETRY DRIVEN BIFURCATION

A. Confrontation experiment theory

Recently, we have reported the observation of a new light-induced bifurcation under CP excitation above the Fréedericksz transition, a bifurcation that was missed in earlier investigations [21]. This transition is well defined in our experiment as a bifurcation point, where the modal composition of the molecular organization is drastically changed. The experimental setup is detailed in Ref. [21]. Figure 8 presents the intensity of the x component, $I_x(t)$, of the light emerging from the sample. For $1<\tilde{I}<\tilde{I}_B$, $I_x(t)$ shows an almost sinusoidal oscillation that corresponds to the three-dimensional quasiuniform precession regime detailed in Sec. III A. At $\tilde{I}=\tilde{I}_B \approx 1.25$ (experimental value), the dynamics of the system changes abruptly, as illustrated in Fig. 8. In Ref. [21], we made a quantitative measurement of the appearance

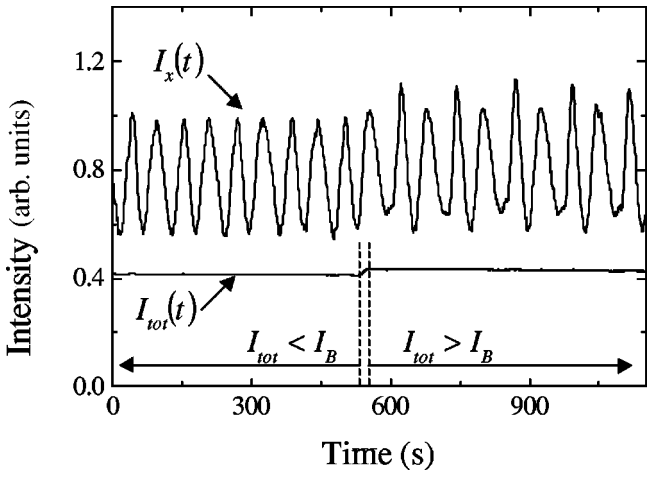

FIG. 8. Experimental intensity of the x component of the light emerging from the sample, and total input intensity, $I_{tot}(t)$, in the CP case when the total intensity passes through the critical value $\tilde{I}=\tilde{I}_B$.

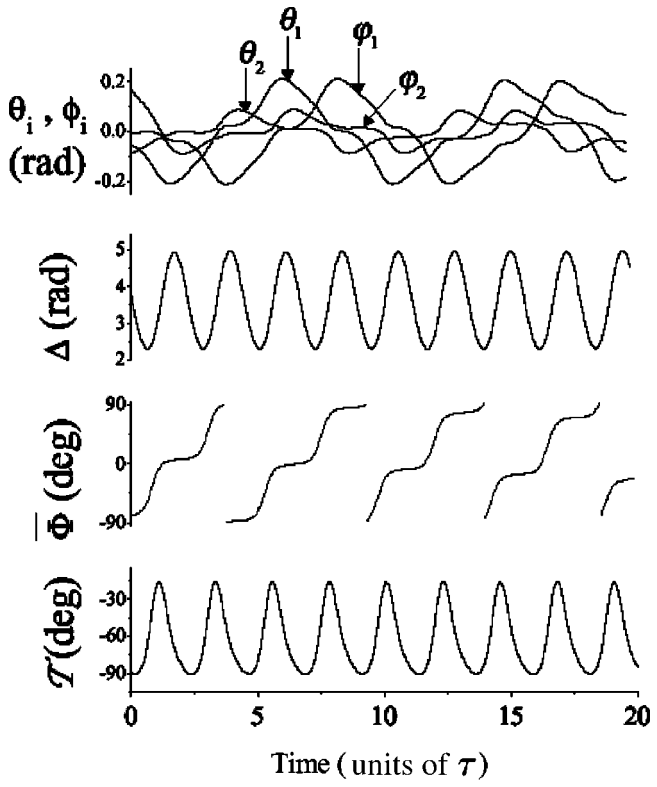

FIG. 9. Nonlinear dynamics calculated at $\tilde{I}=1.9>\tilde{I}_B$ in the CP case. The amplitudes θ_1, θ_2, ϕ_1, and ϕ_2, the position of the averaged plane of reorientation of the molecules $\bar{\Phi}$, the phase shift Δ, and the twist $\mathcal{T}$ are plotted vs time (in units of τ).

of a second dominant frequency and the comparison of experimental data with theory indicated that even at the level of the two-mode approximation (Sec. II C), the model had captured the essential features found in the experiment.

The comparison of Figs. 5 and 9 emphasizes quantitatively the drastic modification of the molecular dynamics at the transition. The three-dimensional dynamics now consists of a nonuniform precession associated with large nutation and torsional oscillations and the transition is accompanied by the appearance of numerous higher-order harmonics of the fundamental frequency for each mode. Figure 10 demonstrates that this transition is unambiguously a bifurcation. This graph presents the trajectories in the phase space $[\tilde{n}_x = \Delta^{1/2}(t)\cos\Phi(L,t), \tilde{n}_y = \Delta^{1/2}(t)\sin\Phi(L,t)]$ where $\tilde{n}_x$ and $\tilde{n}_y$ are proportional to the x and y components of the director, n_x and n_y, at small Θ angles at the exit of the sample. Since the phase portrait changes its topological structure as the intensity passes through the critical value $\tilde{I}=\tilde{I}_B \approx 1.75$ (theoretical value) we conclude that a bifurcation has occurred, the system passing from a periodic regime to quasiperiodicity (Fig. 10). The second-order character of such a bifurcation is further evidenced in Fig. 11, where the maxima of the mode amplitudes, $\alpha_i^{\max} \equiv \max_t |\alpha_i(t)|$, are plotted as function of $\tilde{I}$. One can further extract from Fig. 11 a physical scenario for the production of the transition. At the Fréedericksz threshold ($\tilde{I}=1$) only the symmetric modes are significantly excited, as expected from the quasi-in-plane configuration

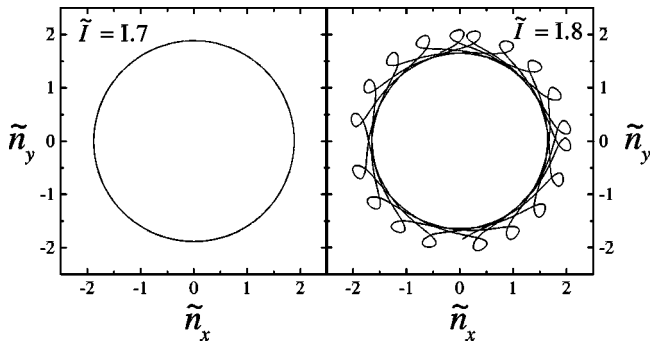

FIG. 10. Trajectories in the phase space $(\tilde{n}_x, \tilde{n}_y)$ in the CP case. The trajectories are plotted for a time interval of 40τ for $\tilde{I}=1.7$ (left) and $\tilde{I}=1.8$ (right).

taken by the NLC molecules at $\tilde{I}=1$ [17,18]. Then, as the light intensity is further increased above threshold, the molecular configuration becomes more and more twisted, thereby associated with significant asymmetry [17,18]. This point is well illustrated in the figure where the contribution of the asymmetric modes to the total reorientation increases almost linearly with the pump intensity up to the critical value $\tilde{I}_B$. Above $\tilde{I}=\tilde{I}_B$, the system is no longer capable to efficiently average the nonuniform spatial deposition of angular momentum and the molecules do not rotate collectively anymore. In other words, some molecules oscillate back and forth as illustrated by the buckles of the phase portrait in Fig. 10 whereas $\bar{\Phi}(t)$ remains monotonic (i.e., positive averaged precession).

Quantitatively, the bifurcation intensity $\tilde{I}_B \approx 1.75$ calculated from the minimal model (Fig. 11) is not in complete agreement with the experimental value $\tilde{I}_{B\text{expt}} \approx 1.25$. Nevertheless, this value remains in a realistic experimental range of light intensity. Part of the remaining discrepancy may be removed by retaining higher-order modes of reorientation.

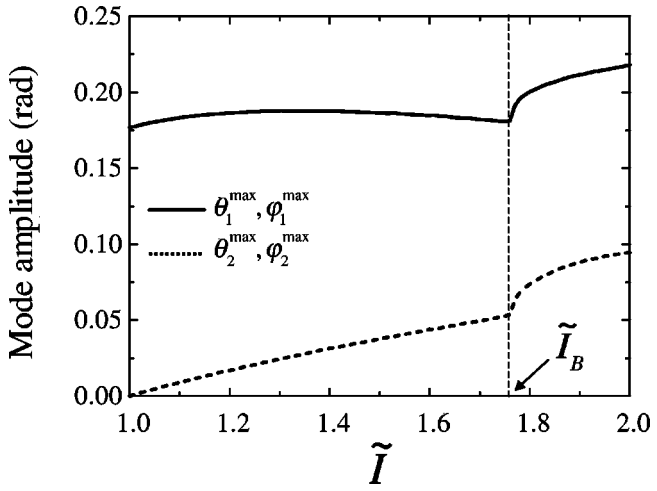

FIG. 11. Theoretical values of maxima of amplitudes $\theta_i^{\max}$ and $\phi_i^{\max}$ $(i=1,2)$ vs the normalized intensity $\tilde{I}$ in the CP case. The solid line represents the symmetric modes (θ_1, ϕ_1) and the dashed line represents the antisymmetric modes $(\theta_2,\ \phi_2)$.

TABLE I. Normalized intensity value of the bifurcation at $\tilde{I}=\tilde{I}_B$ vs the number of reorientation modes in the CP case. For comparison, the experimental value is ~ 1.25.

Number of modes	$\tilde{I}_B$
2	1.75
3	1.47
4	1.44
5	1.44

Table I summarizes the value of $\tilde{I}_B$ in function of the numbers of modes retained in the calculation for each angles θ and ϕ. It is sufficient to consider four modes to reduce the relative discrepancy between theory and experiment from 40% to 15%. We must add that the additional modes do not change the qualitative features of the dynamics presented for the minimal ''two-mode model.'' We should mention that the experimental anchoring conditions are likely to be weaker than the conditions assumed for the model. The case of finite anchoring might be treated in first approximation using an effective cell thickness slightly larger than L and keeping the strong anchoring conditions at the border of the effective cell. However, small thickness variation cannot explain the residual discrepancy in the weakly reoriented regime ($\Delta \approx \pi$). At present, we believe that the answer could be found in the experimental finite beam size and this would imply the necessity to develop an appropriate theoretical improvement of the model.

B. Qualitative interpretation

The model predicts another interesting feature that identifies a threshold $\tilde{I}=\tilde{I}_B$. When the unperturbed NLC is *abruptly* excited with intensity $\tilde{I}<\tilde{I}_B$, the system settles in a weakly reoriented regime ($\Delta \approx \pi$) after an oscillatory damped transient (Fig. 12). This final state is identical to the one that would have been obtained by a slow increase of intensity from 0 to the same $\tilde{I}$. On the contrary, applying the same procedure for $\tilde{I}>\tilde{I}_B$, the final state is then strongly reoriented ($\Delta \gg 1$, see Fig. 12) although stable orbits with $\Delta \approx \pi$ do exist in that region and are, as in the previous case, reached through a slow increase of intensity. The role of twisted reorientation mode in the optical phase locking above the Fréedericksz transition pointed out in Sec. III A suggests that the competition between the growth rate of polar (Θ) and azimuthal (Φ) reorientation modes is at the origin of the phenomenon.

To clarify this point, let us introduce the characteristic times of reorientation τ_Θ and τ_Φ that correspond to the angles Θ and Φ, respectively, and define the ratio $r=\tau_\Theta/\tau_\Phi$. We may also recall that Θ is directly linked to the amplitude of the reorientation ($\Delta \propto \Theta^2$ in the limit $\Theta^2 \ll 1$) and Φ defines the twisted character of the molecular organization. When $r>1$ the twisted deformations first take place. Part of the *e*-waves energy is transferred to the *o*-wave due to nonadiabatic propagation which limits the reorientation am-

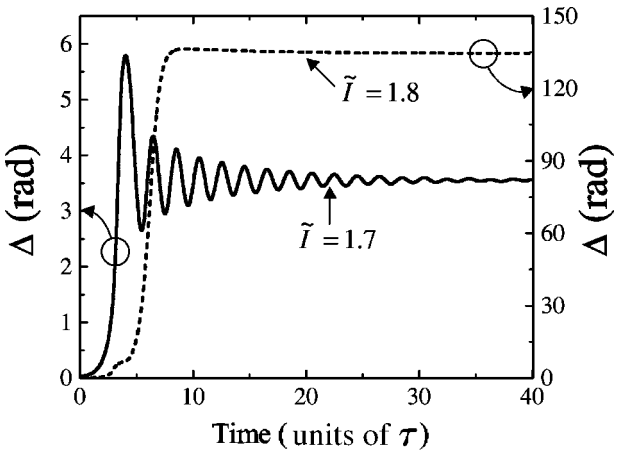

FIG. 12. Transient regime $\Delta(t)$ vs time (in units of τ) in the CP case. Initial conditions are $\theta_i=\phi_i=10^{-2}$ $(i=1,2)$. The black line corresponds to $\tilde{I}=1.7<\tilde{I}_B$ and the dashed line corresponds to $\tilde{I}=1.8>\tilde{I}_B$.

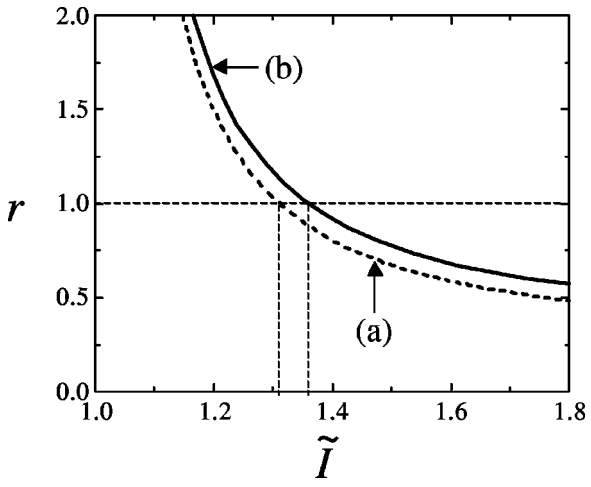

FIG. 13. Ratio $r=\tau_\Theta/\tau_\Phi$ calculated in the CP case in the limit of small reorientation. (a) The deformations are assumed to have the form $\Theta(z)=\Theta_0\sin(\pi z/L)$ and $\Phi(z,t)=\Omega t+\alpha(z)$ [19,27]. (b) The deformations are assumed to have the form $\Theta(z)=\Theta_0\sin(\pi z/L)$, $\Phi(z,t)=\Phi_0(t)+\Phi_1\cos(\pi z/L)$ [20].

plitude and this corresponds to the case $\tilde{I}<\tilde{I}_B$. Inversely, if $r<1$ the polar deformations take place more rapidly than the twist. Then the transient reorientation is quasi-in-plane and the final state is strongly reoriented; this is the case $\tilde{I}>\tilde{I}_B$. Thus, the condition $r=1$ allows us to define $\tilde{I}_B$. Since $\tau_\Theta=\tau/(\tilde{I}-1)$ and $\tau_\Phi=\tau\Delta/\tilde{I}$ [28] when the final state is defined by $(\Delta,\tilde{I})$, $\tilde{I}_B$ is the solution of the transcendental equation, $\Delta(\tilde{I})(\tilde{I}-1)-\tilde{I}=0$. As illustrated in Fig. 13, where r is plotted versus $\tilde{I}$ in two situations that admit an analytical stationary solution $\Delta(\tilde{I})$ [19,20,27], we obtain typically $\tilde{I}_B\approx1.3$–1.35 in rather good agreement with the experimental value $\tilde{I}_{B\text{expt}}\approx1.25$.

V. TWIST DRIVEN OPTICAL BISTABILITY

A. Confrontation experiment theory

When the unperturbed NLC is *gradually* excited with CP or CP$^\pm$ light fields, reorientation occurs at $\tilde{I}=1$ and the system is phase locked with $\Delta\approx\pi$ until an abrupt transition to a strongly reoriented state with $\Delta\gg1$ appears at $\tilde{I}=\tilde{I}^*$. Figures 14 and 15 present the experimental phase shift Δ versus the normalized intensity for CP and CP$^\pm$ excitations, respectively. The transition at $\tilde{I}=\tilde{I}^*$ is observed at lower intensity in the CP case, where $\tilde{I}^*_{CP\text{expt}}\approx1.45$ (Fig. 14), than in the CP$^\pm$ case where $\tilde{I}^*_{\text{CP}^\pm\text{expt}}\approx1.6$ (Fig. 15). Experimentally, such a transition is unambiguously identified with the sudden appearance of a large number of diffraction rings which are the result of self-focusing due to the finite beam size [29]. In addition, both in CP and CP$^\pm$ excitations, the NLC is still strongly reoriented even if the intensity is reduced below $\tilde{I}^*$ that concludes to a first-order transition with large hysteresis (Figs. 14 and 15). As seen from the figures, agreement between theory and experiment is good since the main observed features are predicted by the model. In particular, the threshold is predicted to be lower in the CP case than in the CP$^\pm$ case, as observed.

Quantitatively, the bifurcation intensities $\tilde{I}^*_{\text{CP}}\approx2.12$ and $\tilde{I}^*_{\text{CP}^\pm}\approx2.26$ calculated from the minimal model are somewhat larger than the experimental ones. Our previous com-

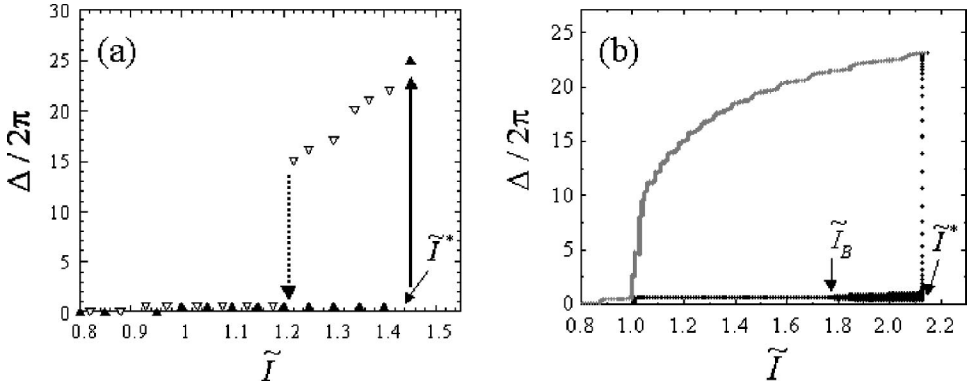

FIG. 14. Reorientation amplitude Δ vs the normalized intensity under CP excitation. (a) Experimental data taken from Ref. [17]. (b) Theory.

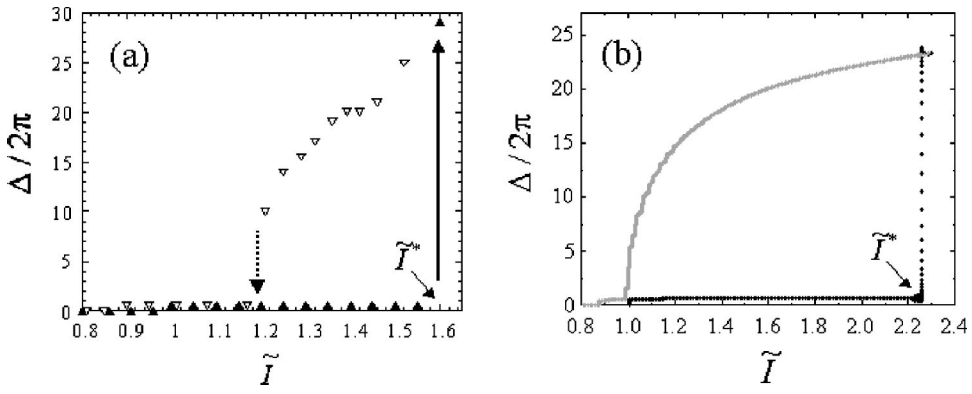

FIG. 15. Reorientation amplitude Δ vs the normalized intensity under $CP^{\pm}$ excitation. (a) Experimental data. (b) Theory.

ment with regards to the discrepancy in $\tilde{I}_B$ applies here also (see Sec. IV). From Table II, which summarizes the value of $\tilde{I}^*$ as a function of the numbers of modes in the CP case, it is enough to retain four modes to reduce the relative discrepancy between theory and experiment from 46% to 21%. However, in the $CP^{\pm}$ case, additional modes do not reduce significantly the threshold.

It is worth mentioning that in previous experimental work we have suggested that such a transition is intimately linked with the existence of a weakly reoriented state with a significantly twisted molecular organization [17]. In particular, this abrupt transition to a large reoriented state is not observed experimentally when the excitation light field is CP^+ [17]. Indeed, such an excitation field induces quasi-in-plane reorientation above the Fréedericksz threshold as predicted in Ref. [17] and observed in Ref. [18]. Figure 16 shows the intensity dependence of Δ in the CP^+ case. The phase locking is absent and no abrupt transition is predicted by the model, in agreement with experiments. It was furthermore demonstrated experimentally that the strongly reoriented state has no significant twist [19] in distinction to the state below $\tilde{I}^*$ and the model agrees also with this observation. It is important to realize that this abrupt increase of the reorientation amplitude at $\tilde{I}=\tilde{I}^*$ results from the sudden *energy transfer from the o wave to the e wave* and not to a release of the elastic energy stored in the twisted reorientation modes. Indeed, when $\tilde{I}<\tilde{I}^*$, the tilt angle θ is small ($\theta \sim 10°$) and it can be shown from Eq. (1) that the relative contribution of the twist deformations to the elastic free energy is proportional to θ^2. The release of the twist elastic energy is therefore insufficient to account for the increase of θ from 10° to many tens of degrees when $\tilde{I}>\tilde{I}^*$.

TABLE II. Normalized intensity value of the bifurcation at $\tilde{I}=\tilde{I}^*$ vs the number of reorientation modes in the CP case. For comparison, the experimental value is ~ 1.45.

Number of modes	$\tilde{I}^*$
2	2.12
3	2.19
4	1.75
5	1.75

Finally, we would like to emphasize that such a mirrorless intrinsic optical bistability is intimately linked to the helical shaped spatial organization of the material and is not restricted to the present work. Indeed, such bistability is also observed in the case of a nematic liquid crystal doped by chiral agents under polarized light excitation [30–32]. Another example is provided when a cholesteric liquid crystal is illuminated with very intense circularly polarized light. In that case the changes of the pitch of the light-induced helix lead to a bistable Bragg reflection [33], which was observed experimentally [34].

B. A dynamical scenario

Figure 17 shows the solution $\Delta(\tilde{I})$, for the CP case, of earlier studies of Zolot'ko and Sukhorukhov [20] (solid line) and Marrucci *et al.* [27] (dashed line), where s_i and u_i refer to stable and unstable branches, respectively. These models succeeded to describe the first-order Fréedericksz transition but failed to explain the transition at $\tilde{I}=\tilde{I}^*$, since the unstable branch u_1 does not coalesce with the stable one s_0 in a saddle-node bifurcation that would have led to a strongly reoriented state. This is because in these models, the system is restricted to a limit cycle behavior corresponding to a uniform precession of the director associated with time-

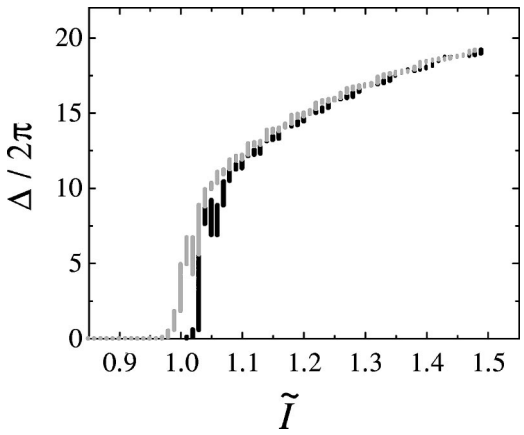

FIG. 16. Theoretical Δ vs the normalized intensity under CP^+ excitation.

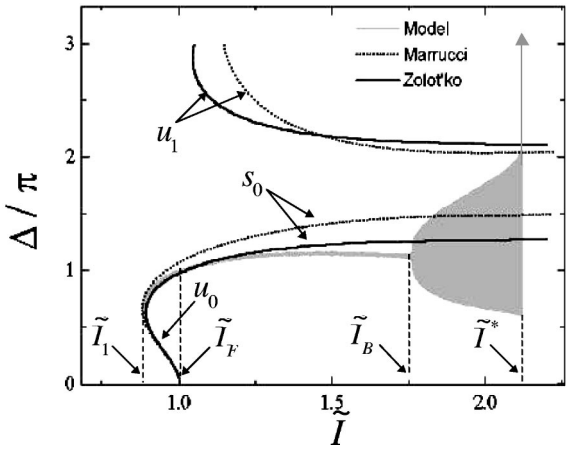

FIG. 17. Theoretical Δ vs the normalized intensity $\tilde{I}$ for small reorientation ($\Delta \leqslant 2\pi$) with different approaches for CP excitation. The model presented in Sec. II appears in gray where the vertical upward arrow indicates that the system switches to a strongly reoriented state when $\tilde{I}=\tilde{I}^*$ (see Fig. 14). The dotted line refers to the model proposed by Marrucci *et al.* [27] and the solid line refers to the model of Zolot'ko and Sukhorukhov [20]. s_i and u_i indicate stable (positive slope) and unstable (negative slope) branches, respectively.

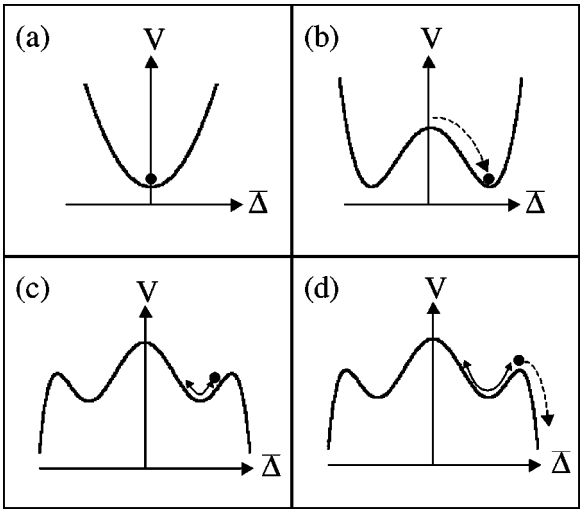

FIG. 18. Phenomenological illustration of the dynamical scenario when the system is gradually excited from the unperturbed state. The NLC state is pictured as a particle sliding on the walls of the light-induced potential $V(\Delta)$. (a) $\tilde{I}<1$, (b) $\tilde{I}=1$, (c) $\tilde{I}=\tilde{I}_B$, and (d) $\tilde{I}=\tilde{I}^*$.

independent three-dimensional molecular spatial organization. A qualitative physical explanation based on dynamic fluctuations of the director was already suggested in Ref. [17]. There, the occurrence of a sufficiently large fluctuation that could initiate the jump over the potential barrier u_1 was discussed. In the present model such fluctuations are allowed. As displayed in Fig. 17 (gray), these fluctuations are born at the second-order bifurcation ($\tilde{I}=\tilde{I}_B$) (Sec. IV) and, at $\tilde{I}=\tilde{I}^*$, they become large enough to initiate the first-order transition to a large reoriented state. Such a scenario can be visualized qualitatively in Fig. 18 where the NLC is pictured as a particle sliding on the walls of a light-induced potential $V(\Delta)$.

VI. CONCLUSION

We have presented a theoretical study of optically induced nonlinear dynamics in nematic liquid crystals in the framework of circularly polarized excitation beams at normal incidence. A minimal four-dimensional model has been introduced that succeeds in describing a wealth of experimental observations such as three-dimensional dynamics in the case of a single circularly polarized beam, light-induced stabilized helical deformations in the case of two incoherent counterpropagating circularly polarized beams with opposite angular momentum and same intensities, and finally in-plane precession regime in the case of two incoherent counterpropagating circularly polarized beams with same angular momentum and intensities.

The longitudinal symmetry breakdown and mode competition have been shown to be at the origin of the second-order transition above the optical Freédericksz transition where the system bifurcates towards a large nutation regime. Moreover, the first quantitative description of the first-order transition with large hysteresis from the phase locked weakly reoriented state to a large reoriented state has been given. The role of twisted reorientation modes and large orientational fluctuations induced by longitudinal nonlocality (elasticity) in the observation of such a transition have been emphasized. The model presented is quite versatile and agreement with experimental data is satisfactory in all cases.

We believe that the *transverse nonlocality* due to the experimental finite beam size and which has been neglected in the present work, could explain residual discrepancies between theory and experiment. Together with the present findings that identify the *longitudinal* nonlocality to be at the origin of a bifurcation missed in earlier investigations, we foresee that a new, not yet observed experimentally, class of light-induced nonlinear dynamics in liquid crystals is yet to be discovered as one starts to probe the effects of *three-dimensional* nonlocality.

[1] N.V. Tabiryan, A.V. Sukhov, and B.Y. Zel'dovich, Mol. Cryst. Liq. Cryst. **136**, 1 (1986).

[2] I.C. Khoo and S.T. Wu, *Optics and Nonlinear Optics of Liquid Crystals* (World Scientific, Singapore, 1993).

[3] E. Santamato, in *Nonlinear Optical Materials and Devices for Applications in Information Technology*, edited by A. Miller *et al.* (Kluwer Academic, Dordrecht, 1995), pp. 103–139.

[4] F. Simoni, *Nonlinear Optical Properties of Liquid Crystals and PDLC* (World Scientific, Singapore, 1997).

[5] A.S. Zolot'ko, V.F. Kitaeva, N. Kroo, N.N. Sobolev, and L.

Csillag, Pis'ma Zh. Eksp. Teor. Fiz. **32**, 170 (1980) [JETP Lett. **32**, 159 (1980)].
[6] A.S. Zolot'ko, V.F. Kitaeva, V. Kuyumchyan, N. Sobolev, A. Sukhorukov, and L. Csillag, Pis'ma Zh. Eksp. Teor. Fiz. **36**, 66 (1982) [JETP Lett. **36**, 80 (1982).
[7] E. Santamato, M. Romagnoli, M. Settembre, B. Daino, and Y.R. Shen, Phys. Rev. Lett. **61**, 113 (1988).
[8] S. Arakelyan, Usp. Fiz. Nauk. **153**, 579 (1987) [Sov. Phys. Usp. **30**, 1041 (1987)].
[9] H.L. Ong, Phys. Rev. A **28**, 2393 (1983).
[10] E. Santamato, G. Abbate, P. Maddalena, L. Marrucci, and Y.R. Shen, Phys. Rev. Lett. **64**, 1377 (1990).
[11] G. Demeter and L. Kramer, Phys. Rev. Lett. **83**, 4744 (1999).
[12] G. Demeter, Phys. Rev. E **61**, 6678 (2000).
[13] G. Demeter and L. Kramer, Phys. Rev. E **64**, 020701 (2001).
[14] G. Russo, V. Carbone, and G. Cipparrone, Phys. Rev. E **62**, 5036 (2000).
[15] V. Carbone, G. Cipparrone, and G. Russo, Phys. Rev. E **63**, 051701 (2001).
[16] A. Vella, B. Piccirillo, and E. Santamato, Phys. Rev. E **65**, 031706 (2002).
[17] E. Brasselet and T.V. Galstian, Opt. Commun. **186**, 291 (2000).
[18] E. Brasselet and T.V. Galstian, Opt. Commun. **200**, 241 (2001).
[19] E. Brasselet and T.V. Galstian, J. Opt. Soc. Am. B **18**, 982 (2001).
[20] A.S. Zolot'ko and A.P. Sukhorukhov, Pis'ma Zh. Eksp. Teor. Fiz. **52**, 707 (1990) [JETP Lett. **52**, 630 (1990).
[21] E. Brasselet, B. Doyon, T.V. Galstian, and L.J. Dubé, Phys. Lett. A **299**, 212 (2002).
[22] P.G. de Gennes and J. Prost, *The Physics of Liquid Crystals*, 2nd ed. (Clarendon Press, Oxford, 1993).
[23] B.Y. Zel'dovich and N. Tabiryan, Zh. Eksp. Teor. Fiz. **82**, 1126 (1982) [Sov. Phys. JETP **55**, 656 (1982)].
[24] D. Berreman, J. Opt. Soc. Am. **62**, 502 (1972).
[25] W.H. Press, S.A. Teukolsky, W.T. Vetterling, and B.P. Flannery, *Numerical Recipes in Fortran 77. The Art of Scientific Computing*, 2nd ed. (Cambridge University Press, Cambridge, 2001).
[26] C. Mauguin, Phys. Z. **12**, 1011 (1911).
[27] L. Marrucci, G. Abbate, S. Ferraiuolo, P. Maddalena, and E. Santamato, Phys. Rev. A **46**, 4859 (1992).
[28] L. Marrucci, P. Maddalena, G. Arnone, L. Sirleto, and E. Santamato, Phys. Rev. E **57**, 3033 (1998).
[29] S.D. Durbin, S.M. Arakelian, and Y.R. Shen, Opt. Lett. **64**, 020701 (1981).
[30] G. Abbate, P. Maddalena, L. Marrucci, L. Saetta, A. Ferraiuolo, and E. Santamato, Mol. Cryst. Liq. Cryst. **223**, 11 (1992).
[31] G. Abbate, A. Ferraiuolo, P. Maddalena, L. Marrucci, and E. Santamato, Liq. Cryst. **14**, 1431 (1993).
[32] P. Maddalena, G. Arnone, G. Abbate, L. Marrucci, and E. Santamato, Mol. Cryst. Liq. Cryst. **261**, 113 (1995).
[33] H.G. Winful, Phys. Rev. Lett. **49**, 1179 (1990).
[34] S. Lukishova, E. Magulariya, and K. Lebedev, Proc. SPIE **2800**, 196 (1996).

Optically Induced Dynamics In Nematic Liquid Crystals:
The Role of Twist Deformation and Asymmetry

E. Brasselet, B. Doyon, T.V. Galstian, and L.J. Dubé

Physical Review E **67**, 031706 (1-13) (2003)

The labels on FIG. 4 have been modified during the production process. Also the symbols ∘ and • have been inverted in the figure caption. Here is the correct version.

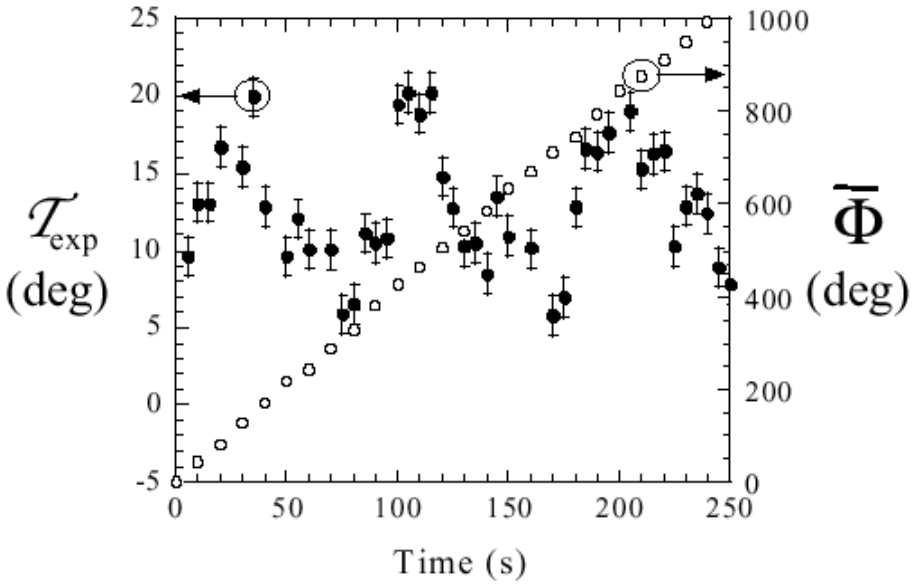

FIG. 4: Experimental demonstration of the torsional oscillation regime coupled with induced precession from Ref. [18] with CP excitation beam. $\tilde{I} \approx 1.1$ and the cell thickness is 90 μm. • twist $\mathcal{T}$; ∘ position of the averaged plane of reorientation of the molecules $\overline{\Phi}$.